

# Eccentric Dynamical Tides

Yubo Su<sup>1</sup>, Dong Lai<sup>1</sup>

<sup>1</sup> *Cornell Center for Astrophysics and Planetary Science, Department of Astronomy, Cornell University, Ithaca, NY 14853, USA*

Accepted XXX. Received YYY; in original form ZZZ

## ABSTRACT

Abstract

**Key words:** keywords

## 1 INTRODUCTION

In the course of their evolution, massive stellar binaries give rise to many astrophysical systems of interest including high mass x-ray binaries (HMXRBs) and compact object binaries (CITATION with evolutionary pathway). In general, the more massive star undergoes a supernova before its less massive companion, after which the binary consists of one massive star and one compact object in an eccentric orbit (MS-CO binary). In such a system, the evolution is dominated by the torque from the compact object on the massive star due to dynamical tides. While this tidal torque is now well understood for circular binaries (Kushnir et al. 2017), it has not been carefully studied for binaries with substantial eccentricities. The tidal evolution of such eccentric binaries sculpt the population of HMXRBs (CITE) as well as the population of compact object binaries (Vigna-Gómez et al. 2020).

The dissipation due to the dynamical tide in a massive star’s envelope under the influence of a circular perturber is traditionally understood via Zahn’s parameterized theory of dynamical tides (Zahn 1975). However, Zahn’s theory relies on a dimensionless parameter  $E_2$  reflecting the detailed stellar structure that varies over many orders of magnitudes for typical stars. In general, the value of  $E_2$  is taken from empirical fits to simplified stellar models (Hurley et al. 2002; Vigna-Gómez et al. 2020). The introduction of this uncertain parameter  $E_2$  is because the dynamical tidal torque arises due to excitation of internal gravity waves at the radiative convective boundary (RCB) (Goldreich & Nicholson 1989; Savonije & Papaloizou 1983), but Zahn’s formula is evaluated at the stellar radius. Instead, it is possible re-express the tidal torque in terms of quantities evaluated at the RCB itself, for which dimensionless parameters are generally of order unity for a wide range of stars (Kushnir et al. 2017). However, Kushnir et al. (2017) only consider circular binaries.

To study the dynamical tide in eccentric binaries, it is natural to decompose the perturbing potential into Fourier harmonics, each of which is analogous to a perturber on a circular orbit (e.g. Storch & Lai 2013; Vick et al. 2017). While accurate, such decompositions are unwieldy to evaluate as the eccentricity increases, often requiring summing hundreds of terms and lending little intuition to the broad scalings of the tidal torque. In this work, we show that, for the circular torque given by Kushnir et al. (2017), an accurate, approximate, closed form for the dynamical tide in a highly eccen-

tric MS-CO binary can be obtained. Contrary to existing models of dynamical tides (e.g. Vigna-Gómez et al. 2020), our formulation improves in accuracy as the binary eccentricity increases. We give closed forms for both the tidal torque and inspiral rate of such an MS-CO binary.

In Section 2, we review the relevant equations. In Section 3, we derive accurate, approximate closed forms for the torque and energy transfer rate in the binary. In Section 4, we apply results to the binary radio pulsar J0045-7319. We conclude and discuss in Section 5.

## 2 SUMMARY OF RELEVANT WORK

### 2.1 Tidal Torque in Massive Stars

We first review the case where the MS-CO binary is circular. Let  $M_2$  be the mass of the CO,  $a$  be the semimajor axis of the binary, and  $\omega$  the orbital angular frequency of the binary. The tidal torque exerted on the star by the companion is traditionally expressed as (Zahn 1975)

$$\tau = \frac{3}{2} \frac{GM_2^2}{R} \left( \frac{R}{d} \right)^6 E_2 s^{8/3}, \quad (1)$$

where  $s = 2|\omega - \Omega_s| \sqrt{R^3/GM}$  pattern frequency of the tide normalized by the breakup rotation rate,  $\Omega_s$  is the spin frequency of the star, and  $E_2$  is a numerical parameter that varies widely depending on stellar properties. (e.g. Hurley et al. (2002) gives  $E_2 = 1.6 \times 10^{-9} (M/M_\odot)^{2.84}$ ).

A more physically motivated formulation of the tidal torque is

given by [Kushnir et al. \(2017\)](#) as

$$\begin{aligned}\tau &= \hat{\tau}(\omega) \operatorname{sgn}\left(1 - \frac{2\Omega_s}{\omega}\right) \left|1 - \frac{2\Omega_s}{\omega}\right|^{8/3}, \\ \hat{\tau}(\omega) &= \frac{GM_c^2 r_c^5}{a^6} \left(\frac{\omega}{\sqrt{GM_c/r_c^3}}\right)^{8/3} \left[\frac{r_c}{g_c} \left(\frac{dN^2}{d \ln r}\right)_{r=r_c}\right]^{-1/3} \\ &\quad \times \frac{\rho_c}{\bar{\rho}_c} \left(1 - \frac{\rho_c}{\bar{\rho}_c}\right)^2 \left[\frac{3}{2} \frac{3^{2/3} \Gamma^2(1/3)}{5 \cdot 6^{4/3}} \frac{3}{4\pi} \alpha^2\right], \\ &\equiv \beta_2 \frac{GM_c^2 r_c^5}{a^6} \left(\frac{\omega}{\sqrt{GM_c/r_c^3}}\right)^{8/3} \frac{\rho_c}{\bar{\rho}_c} \left(1 - \frac{\rho_c}{\bar{\rho}_c}\right)^2.\end{aligned}\quad (2)$$

Here,  $N$  is the Brünt-Vaisala frequency,  $r$  is the radial coordinate within the star, and  $r_c$ ,  $M_c$ ,  $g_c$ ,  $\rho_c$ ,  $\bar{\rho}_c$  are the radius of the RCB, the mass contained within the convective core, the gravitational acceleration at the RCB, the stellar density at the RCB, and the average density of the convective core, respectively.  $\alpha$  and  $\beta_2$  are numerical constants defined by [Kushnir et al. \(2017\)](#), where  $\beta_2 \approx 1$  is a good approximation for a large range of stellar models. In Eq. (2), we have written the terms such that  $\hat{\tau}$  is the torque when the MS is non-spinning.

## 2.2 Perturbation from an Eccentric Companion: Hansen Coefficients

Separately, we review the general procedure for calculating tidal dissipation due to an eccentric perturber. The gravitational potential of an eccentric companion can be decomposed at quadrupolar order as a sum over circular orbits ([Storch & Lai 2013](#); [Vick et al. 2017](#)):

$$U = \sum_m U_{2m}(\vec{r}, t), \quad (4)$$

$$\begin{aligned}U_{2m}(\vec{r}) &= -\frac{GM_2 W_{2m} R^2}{D(t)^3} e^{-imf(t)} Y_{2m}(\theta, \phi), \\ &= -\frac{GM_2 W_{2m} R^2}{a^3} Y_{2m}(\theta, \phi) \sum_{N=-\infty}^{\infty} F_{Nm} e^{-iN\Omega t},\end{aligned}\quad (5)$$

$$F_{Nm} = \frac{1}{\pi} \int_0^\pi \frac{\cos[N(E - e \sin E) - mf(E)]}{(1 - e \cos E)^2} dE. \quad (6)$$

Here,  $R$  is the radius of the star,  $W_{2\pm 2} = \sqrt{3\pi/10}$ ,  $W_{2\pm 1} = 0$ ,  $W_{20} = -\sqrt{\pi/5}$ ,  $D(t)$  is the instantaneous distance between the star and companion,  $f$  is the true anomaly,  $Y_{lm}$  denote the spherical harmonics, and  $\Omega$  is the mean motion of the companion.  $F_{Nm}$  denote are the *Hansen coefficients* for  $l = 2$  (also denoted  $X_{2m}^n$  in [Murray & Dermott 1999](#)).

By considering the effect of each summand in Eq. (5), the total torque on the star, energy transfer in the inertial frame, and heating in the star's corotating frame can be obtained ([Storch & Lai 2013](#);

[Vick et al. 2017](#)):

$$\tau = \sum_{N=-\infty}^{\infty} F_{N2}^2 \hat{\tau}(\omega = N\Omega - 2\Omega_s), \quad (7)$$

$$\begin{aligned}\dot{E}_{\text{in}} &= \frac{1}{2} \sum_{N=-\infty}^{\infty} \left\{ \left(\frac{W_{20}}{W_{22}}\right)^2 N\Omega F_{N0}^2 \hat{\tau}(\omega = N\Omega) \right. \\ &\quad \left. + N\Omega F_{N2}^2 \hat{\tau}(\omega = N\Omega - 2\Omega_s) \right\},\end{aligned}\quad (8)$$

$$\dot{E}_{\text{rot}} = \dot{E}_{\text{in}} - \Omega_s \tau, \quad (9)$$

where  $\hat{\tau}(\omega)$  is the torque exerted by a perturber on a circular trajectory with orbital frequency  $\omega$ . Our notation differs from that of [Vick et al. \(2017\)](#), where we write  $\hat{\tau}(\omega) = T_0 \operatorname{sgn}(\omega) \hat{F}(|\omega|)$  in their notation, to easier incorporate the results of the previous section.

## 2.3 Objective of This Paper

The objective of this paper is to study the effect of dynamical tides in an eccentric MS-CO binary. First, we compute the tidal torque by substituting the torque due to a CO on a circular orbit [Eq. (2)] into the summation Eq. (7), obtaining

$$\tau = \sum_{N=-\infty}^{N=\infty} F_{N2}^2 \hat{\tau}(\Omega) \operatorname{sgn}\left(N - \frac{2\Omega_s}{\Omega}\right) \left|N - \frac{2\Omega_s}{\Omega}\right|^{8/3}. \quad (10)$$

The energy transfer rate in the inertial frame is similarly obtained by substituting Eq. (2) into Eq. (8)

$$\begin{aligned}\dot{E}_{\text{in}} &= \frac{\hat{\tau}(\Omega)}{2} \sum_{N=-\infty}^{\infty} \left[ N\Omega F_{N2}^2 \operatorname{sgn}(N - 2\Omega_s/\Omega) |N - 2\Omega_s/\Omega|^{8/3} \right. \\ &\quad \left. + \left(\frac{W_{20}}{W_{22}}\right)^2 \Omega F_{N0}^2 |N|^{11/3} \right].\end{aligned}\quad (11)$$

These two expressions give the spin synchronization timescale of the star as well as the inspiral time of the binary due to dynamical tides. While exact, these expressions give little insight when the eccentricity is substantial, as one often must sum hundreds or thousands of terms, each of which has a different  $F_{Nm}$ . In the subsequent sections, our objective is to obtain closed-form approximations to Eqs. (10–11).

## 3 EVALUATING TORQUE AND ENERGY TRANSFER

### 3.1 Hansen Coefficient Approximations

Recall that the Hansen coefficients are defined as the Fourier series coefficients of part of the companion's gravitational potential

$$\frac{a^3}{D(t)^3} e^{-imf} = \sum_{N=-\infty}^{\infty} F_{Nm} e^{-iN\Omega t}. \quad (12)$$

Observe that  $F_{(-N)m} = F_{Nm}$ , so we will only study the Hansen coefficient behavior for  $m \geq 0$ .

#### 3.1.1 $m = 2$ Hansen Coefficient Behavior

We first consider the case where  $m = 2$ . We give an example of the behavior of the  $F_{N2}$  for  $e = 0.9$  in Fig. 1, and make the following observations:

- $F_{N2}$  is much larger for  $N \geq 0$  than for  $N < 0$ .

• For  $N \geq 0$ ,  $F_{N2}$  has only one substantial peak. The only characteristic scale for  $N$  is the pericenter harmonic

$$N_p \equiv \lfloor \Omega_p / \Omega \rfloor, \quad (13)$$

where  $\Omega_p$  is the pericenter frequency, defined by

$$\Omega_p \equiv \Omega \frac{\sqrt{1+e}}{(1-e)^{3/2}}. \quad (14)$$

Thus, we expect that the peak of the  $F_{N2}$  should occur at  $\sim N_p$ , which is indeed the case.

• Since the left hand side of Eq. (12) is smooth, the Fourier coefficients must fall off exponentially for  $N \gg N_p$  by the Paley-Wiener theorem.

• Since there are no characteristic timescales between  $\Omega$  and  $\Omega_p$ , we anticipate the Hansen coefficients must be scale free between  $N = 1$  and  $N_p$ , i.e. a power law.

Motivated by these considerations, we assume the Hansen coefficients can be approximated by

$$F_{N2} \approx \begin{cases} C_2 N^p e^{-N/\eta_2} & N \geq 0, \\ 0 & N < 0, \end{cases} \quad (15)$$

for some fitting coefficients  $C_2$ ,  $p$ , and  $\eta_2$ . By performing fits to  $F_{N2}$ , we found that  $p \approx 2$  is relatively constant for modest-to-large large eccentricities. This is expected, as the left hand side of Eq. (12) resembles the second derivative of a Dirac delta for  $N \lesssim N_p$  when the eccentricity is substantial<sup>1</sup>. For the remainder of this work, we take  $p = 2$  to be fixed.

To constrain the remaining two free parameters  $\eta_2$  and  $C_2$  the normalization, we use the well known Hansen coefficient moments (Hut 1981)

$$\sum_{N=-\infty}^{\infty} F_{N2}^2 = \frac{1 + 3e^2 + 3e^4/8}{(1-e^2)^{9/2}} \equiv \frac{f_5}{(1-e^2)^{9/2}}, \quad (16)$$

$$\begin{aligned} \sum_{N=-\infty}^{\infty} F_{N2}^2 N &= \frac{2}{(1-e^2)^6} \left( 1 + \frac{15e^2}{2} + \frac{45e^4}{8} + \frac{5e^6}{16} \right) \\ &\equiv \frac{2f_2}{(1-e^2)^6}. \end{aligned} \quad (17)$$

This fixes

$$\eta_2 = \frac{4f_2}{5f_5(1-e^2)^{3/2}}, \quad (18)$$

$$C_2^2 \eta_2^5 = \frac{4f_5}{3(1-e^2)^{9/2}}. \quad (19)$$

This parameterization is compared to explicit evaluation of the Hansen coefficients in Fig. 1. The agreement is particularly striking as this parameterization uses zero free parameters.

<sup>1</sup> Note that the left hand side of Eq. (12) is sharply peaked about  $t = 0$ , is periodic with period  $P = 2\pi/\Omega$ , and has zero derivative three times every period (at  $t = \epsilon$ ,  $t = P/2$ , and  $t = P - \epsilon$  for some small  $\epsilon \sim 1/\Omega_p$ ). This characteristics imply that it can be well approximated by the second derivative of a Gaussian with width  $\sim 1/\Omega_p$ . For frequencies  $\Omega \lesssim \Omega_p$ , this Gaussian is further well approximated by a Dirac delta, which has a flat Fourier transform ( $\propto N^0$ ). Since time differentiation multiplies by  $N$  in frequency space, we see indeed that  $F_{N2} \propto N^2$  for  $N \lesssim N_p$ .

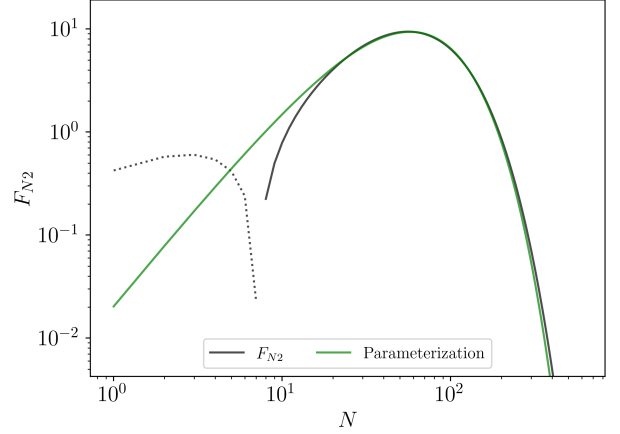


**Figure 1.** Plot of Hansen coefficients  $F_{N2}$  for  $e = 0.9$ , where dotted line denotes negative values. The green line is the parameterization of Eq. (15) with  $\eta_2$  and  $C_2$  given by Eqs. (18–19).

### 3.1.2 $m = 0$ Hansen Coefficient Behavior

We now turn to the case where  $m = 0$  in Eq. (12). These coefficients also only have one characteristic scale in harmonic space ( $N_p$ ), but are also symmetric. Therefore, the natural ansatz is of form

$$F_{N0} = C_0 e^{-|N|/\eta_0}. \quad (20)$$

The two free parameters  $C_0$  and  $\eta_0$  are again constrained by the well known moments (Hut 1981)

$$\sum_{N=-\infty}^{\infty} F_{N0}^2 = \frac{f_5}{(1-e^2)^{9/2}}, \quad (21)$$

$$\sum_{N=-\infty}^{\infty} F_{N0}^2 N^2 = \frac{9e^2}{2(1-e^2)^{15/2}} f_3. \quad (22)$$

This fixes

$$\eta_0^2 = \frac{9e^2 f_3}{(1-e^2)^3 f_5}, \quad (23)$$

$$C_0^2 \eta_0 = \frac{f_5}{(1-e^2)^{9/2}}. \quad (24)$$

## 3.2 Evaluating Torque and Energy Transfer

We now return to the summations in Section 2.3 and simplify them using the parameterized Hansen coefficients from the previous section.

### 3.2.1 Tidal Torque

We return now to Eq. (10). By replacing the  $F_{N2}$  coefficients with Eq. (15) and approximating the sum with an integral, we obtain

$$\tau = \hat{\tau}(\Omega) \int_0^\infty C_2^2 N^4 e^{-2N/\eta_2} \operatorname{sgn}(N - 2\Omega_s/\Omega) |N - 2\Omega_s/\Omega|^{8/3} dN. \quad (25)$$

This can be further simplified. Define  $N_{\max} = 10\eta_2/3$  to be the  $N$  for which the integrand in Eq. (25) is largest assuming  $\Omega_s = 0$  (if  $|\Omega_s|$  is large, the integrand is instead maximized at

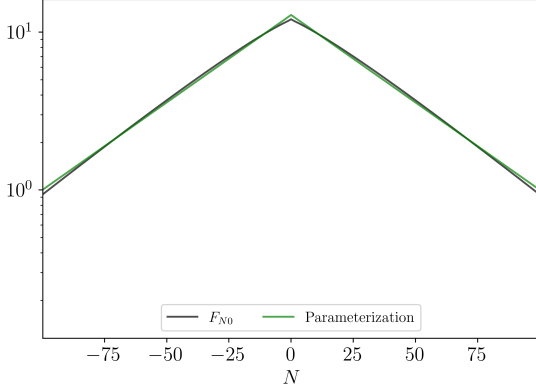


**Figure 2.** Plot of  $F_{N0}$  for  $e = 0.9$ . The green line denotes the parameterization of Eq. (20) with  $\eta_0$  and  $C_0$  given by Eqs. (23–24).

$N = 2\eta_2 \approx N_{\max}$ ). We first consider the high-spin limit where  $|\Omega_s| \gg N_{\max}\Omega/2$ . In this limit,  $|N - 2\Omega_s/\Omega| \approx 2\Omega_s/\Omega$ , and the sum in Eq. (10) can be evaluated directly with the known Hansen coefficient moment in Eq. (16)

$$\lim_{\Omega_s \rightarrow \infty} \tau = -\hat{\tau}(\Omega) \operatorname{sgn}(\Omega_s) |2\Omega_s/\Omega|^{8/3} \frac{f_5}{(1-e^2)^{9/2}}. \quad (26)$$

If instead the spin is negligible, i.e.  $|\Omega_s| \ll N_{\max}\Omega/2$ , then the summand in Eq. (10) is of form  $\sim F_{N2}^2 N^{8/3}$ . Such a sum cannot be evaluated using the known Hansen coefficient moments, but the integral approximation in Eq. (25) can be readily evaluated (since  $\int_0^\infty x^p e^{-x} dx = \Gamma(p+1)$ ) to yield

$$\lim_{\Omega_s \rightarrow 0} \tau = \hat{\tau}(\Omega) \frac{f_5(\eta_2/2)^{8/3}}{(1-e^2)^{9/2}} \frac{\Gamma(23/3)}{4!}. \quad (27)$$

To obtain a single expression valid in both of these limits, we make the ansatz that  $N - 2\Omega_s/\Omega$  in Eq. (25) can be approximated by

$$N - 2\Omega_s/\Omega \approx \frac{N}{N_{\max}} \left( N_{\max} - \frac{2\gamma_\tau \Omega_s}{\Omega} \right), \quad (28)$$

for some free parameter  $\gamma_\tau$ . Then, Eq. (25) can be integrated analytically, and  $\gamma_\tau$  is constrained by requiring our expression reproduce Eqs. (26–27) in their respective limits. This yields the expression

$$\tau = \hat{\tau}(\Omega) \frac{f_5(\eta_2/2)^{8/3}}{(1-e^2)^{9/2}} \operatorname{sgn} \left( 1 - \gamma_\tau \frac{\Omega_s}{\eta_2 \Omega} \right) \left| 1 - \gamma_\tau \frac{\Omega_s}{\eta_2 \Omega} \right|^{8/3} \frac{\Gamma(23/3)}{4!}, \quad (29)$$

$$\gamma_\tau = 4 \left( \frac{4!}{\Gamma(23/3)} \right)^{3/8} \approx 0.691. \quad (30)$$

Figures 3 and 4 demonstrate the accuracy of this prediction. As expected from the construction of this approximation, both the low and high spin limits are well captured, and the scaling for intermediate spins is also somewhat accurate.

### 3.2.2 Pseudosynchronization

Eq. (29) shows that there is a single  $\Omega_s$  for which the torque  $\tau$  vanishes. This is the pseudosynchronized spin frequency, given by

$$\frac{\Omega_{s,ps}}{\Omega} = \frac{\eta_2}{\gamma_\tau} = \frac{4f_2}{5\gamma_\tau f_5 (1-e^2)^{3/2}}. \quad (31)$$

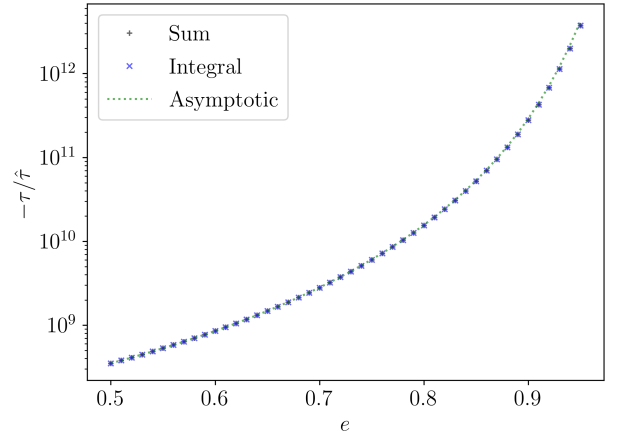
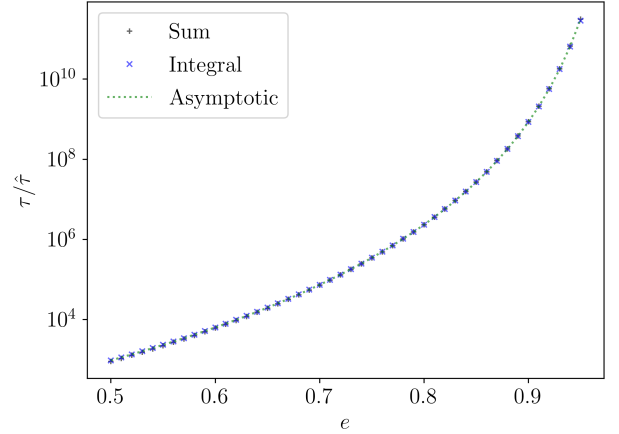


**Figure 3.** Tidal torque on a non-rotating (top) and rapidly rotating ( $\Omega_s/\Omega = 400$ ; bottom) star with a companion having orbital eccentricity  $e$ . Blue plus signs represent explicit summation of Eq. (10), blue crosses are evaluated using the integral approximation Eq. (25), and the green dashed line is Eq. (29).

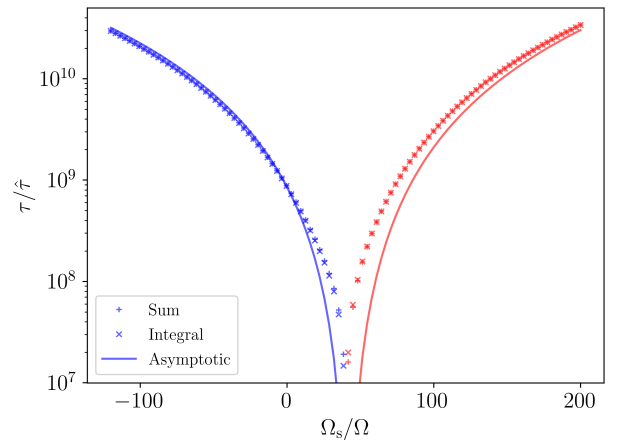


**Figure 4.** Tidal torque as a function of spin for a highly eccentric  $e = 0.9$  companion. Pluses represent direct summation of Hansen coefficients, crosses represent the integral approximation, and solid lines represent the analytic closed form. Blue [red] means positive [negative] torque on the star.

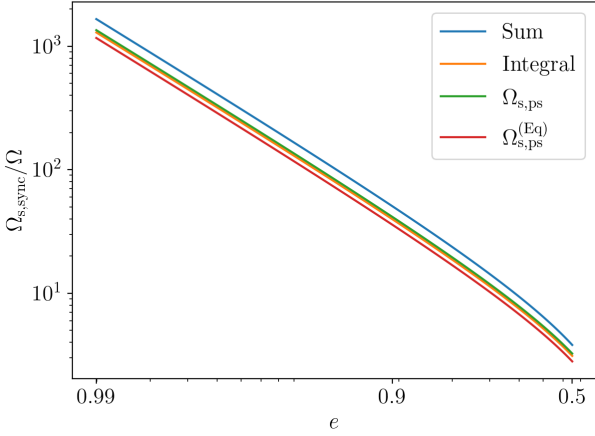


**Figure 5.** Pseudosynchronization frequency computed using the explicit Hansen coefficient sum [Eq. (10); orange], the integral approximation [Eq. (25); blue], our the closed form [Eq. (31); green], and the prediction from weak tidal friction [Eq. (32); red]. We see that Eq. (31) is a very good approximation.

This has the expected scaling  $\Omega_{s,ps} \propto (1 - e^2)^{-3/2}$ , but is more accurate than  $\Omega_{s,ps} \approx \Omega_p$ , as seen in Fig. 5. By comparison, in the standard weak friction theory of equilibrium tides, the pseudosynchronized spin frequency is given by (Alexander 1973; Hut 1981)

$$\frac{\Omega_{s,ps}^{(Eq)}}{\Omega} = \frac{f_2}{f_5 (1 - e^2)^{3/2}}. \quad (32)$$

This differs from our Eq. (31) by a factor of  $\approx 1.15$ .

Note that, very near the pseudosynchronized spin frequency, Eq. (29) predicts that  $d\tau/d\Omega_s \approx 0$ . This is incorrect and is an artifact of our ansatz in Eq. (35). However, reproducing the derivative of the torque requires a more complex parameterization, which we forego in the interest of a simpler asymptotic form that is still accurate except very near pseudosynchronization.

### 3.2.3 Closed Form for Energy Transfer

To compute the energy transfer rate in the inertial frame, we return to Eq. (11) and replace  $F_{N2}$  and  $F_{N0}$  with their approximations Eqs. (15, 20) to obtain

$$\begin{aligned} \dot{E}_{in} = & \frac{\hat{\tau}\Omega}{2} \int_0^\infty \left[ C_2^2 N^5 e^{-2N/\eta_2} \text{sgn}(N - 2\Omega_s/\Omega) |N - 2\Omega_s/\Omega|^{8/3} \right. \\ & \left. + 2 \left( \frac{W_{20}}{W_{22}} \right)^2 C_0^2 e^{-2N/\eta_0} N^{11/3} \right] dN. \end{aligned} \quad (33)$$

We evaluate the  $m = 2$  and  $m = 0$  components of this expression separately.

We first examine the  $m = 2$  contribution using a very similar procedure to what we used for the torque. Again, we define  $N_{\max} = 23\eta_2/6$  the  $N$  for which the integrand is maximized. The high spin limit  $\Omega_s \gg N_{\max}\Omega/2$  comes out to be

$$\lim_{\Omega_s \rightarrow \infty} \dot{E}_{in}^{(m=2)} = -\frac{\hat{\tau}\Omega}{2} \text{sgn}(\Omega_s) |2\Omega_s/\Omega|^{8/3} \frac{2f_2}{(1 - e^2)^6}. \quad (34)$$

We then consider the low-to-moderate spin limit and factorize

$$N - 2\Omega_s/\Omega \approx \frac{N}{N_{\max}} \left( N_{\max} - \frac{2\gamma_E \Omega_s}{\Omega} \right), \quad (35)$$

where  $\gamma_E$  is a free parameter. This lets us integrate Eq. (33) analytically, and we can constrain  $\gamma_E$  by requiring the integral agree with Eq. (34). We obtain that

$$\begin{aligned} \dot{E}_{in}^{(m=2)} = & -\frac{\hat{\tau}\Omega f_5 (\eta_2/2)^{11/3} \Gamma(26/3)}{2(1 - e^2)^{9/2} 4!} \\ & \times \text{sgn} \left( 1 - \gamma_E \frac{\Omega_s}{\eta_2 \Omega} \right) \left| 1 - \gamma_E \frac{\Omega_s}{\eta_2 \Omega} \right|^{8/3}, \end{aligned} \quad (36)$$

$$\gamma_E = \left( \frac{5! 2^{16/3}}{\Gamma(26/3)} \right)^{3/8} \approx 0.5886. \quad (37)$$

The  $m = 0$  contribution to Eq. (33) is much more straightforward and can be directly integrated using the parameterization Eq. (20). We finally obtain the total energy transfer rate

$$\begin{aligned} \dot{E}_{in} = & -\frac{\hat{\tau}\Omega}{2} \left[ \frac{f_5 (\eta_2/2)^{11/3} \Gamma(26/3)}{(1 - e^2)^{9/2} 4!} \right. \\ & \times \text{sgn} \left( 1 - \gamma_E \frac{\Omega_s}{\eta_2 \Omega} \right) \left| 1 - \gamma_E \frac{\Omega_s}{\eta_2 \Omega} \right|^{8/3} \\ & \left. + \frac{f_5 \Gamma(14/3)}{(1 - e^2)^{10}} \left( \frac{3}{2} \right)^{8/3} \left( \frac{e^2 f_3}{f_5} \right)^{11/6} \right]. \end{aligned} \quad (38)$$

We make plots in the two  $\Omega_s$  regimes as a function of eccentricity in Fig. 6 and 7. Agreement is good again.

## 4 EXAMPLE SYSTEM: J0045+7319

We study J0045+7319 (Bell et al. 1995).

We can arrive at an upper bound for the  $\dot{P}$  by setting the spin frequency equal to the breakup frequency. Then, taking the correct parameters and evaluating  $\dot{E}_{in}$ , we obtain

$$\frac{\dot{P}}{2\pi} \lesssim -\frac{3}{(1 + q)^2} \beta_2 \left( \frac{r_c}{a} \right)^5 \frac{\rho_c}{\bar{\rho}_c} \left( 1 - \frac{\rho_c}{\bar{\rho}_c} \right)^2 2^{8/3} \frac{f_2}{(1 - e^2)^6}. \quad (39)$$

This comes out to be  $r_c \gtrsim 1.799 R_\odot$  for J0045+7319, larger than the prior values in the literature and much larger than MESA models.

### 4.1 Stellar Structure Simulations

In previous literature, the primary star was initially taken to have  $M_1 = 8.8 M_\odot$  (Kumar & Quataert 1998; Lai 1996), by taking  $M_2 \approx 1.4 M_\odot$  characteristic mass for NSs and multiplying by the observed  $q$ . A later, but still very old, study proposed  $M_1 \approx 10 M_\odot$  by comparison with stellar models. Using MESA to generate updated stellar models (TODO all citations), we compute an updated  $M_1$  estimate, giving detailed stellar structure measurements.

At the level of approximation of this paper, our procedure is as follows: we use a few different values of convective overshooting and mixing, and metallicities, and compute stellar structures for both non-rotating and highly rotating  $\sim 0.95 \Omega_{s,c}$  stars. We find that, in general, to match the observed  $T, L$  we must let the star evolve to  $\sim 80\%$  of the way to complete core hydrogen depletion. We then sample a range of stellar masses, and find the stellar mass that best reproduces the observed  $T, L$ .

For all of these systems,  $r_c \lesssim R_\odot$ , in tension with our bound above.

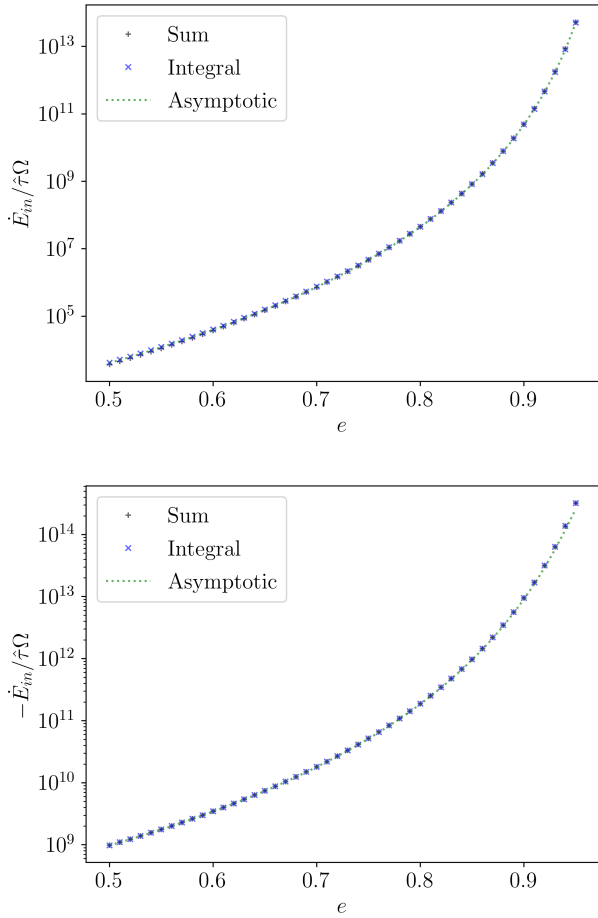


**Figure 6.** Plot of  $\dot{E}_{in}$  for a non-rotating (top) and rapidly rotating ( $\Omega_s/\Omega = 400$ ; bottom) star. Blue pluses represent explicit summation of the Hansen coefficients, crosses the integral form Eq. (33), and the green dashed line the closed form Eq. (38).

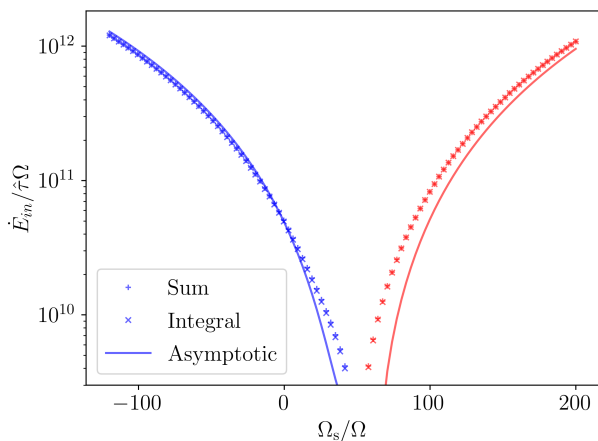


**Figure 7.**  $\dot{E}_{in}$  as a function of spin for a highly eccentric  $e = 0.9$  companion. Pluses represent direct summation of Hansen coefficients, crosses represent the integral approximation, and solid lines represent the analytic closed form. Blue [red] means positive [negative] energy transfer into the stellar spin.

## 5 CONCLUSION AND DISCUSSION

The primary results of the paper is Eq. (29), shown in Figs. 3 and 4 to be accurate across a range of spins and eccentricities. The energy dissipation rate is also computed using similar techniques and show good agreement (see Figs. 6 and 7).

- Thanks to some references (Barker & Ogilvie, my work), there seems to be some evidence that hydrodynamic wave breaking could cause all IGW to break and not reflect, once the pericenter wave reaches nonlinear amplitudes.

- As noted in the text, the approximate forms enforce  $d\tau/d\Omega_s = 0$ , which the actual torque does not satisfy. This introduces some slight errors in the exact value of the torque very near pseudosynchronization.

## 6 ACKNOWLEDGEMENTS

We thank Michelle Vick and Christopher O’Connor for fruitful discussions. YS is supported by the NASA FINESST grant 19-ASTRO19-0041.

## REFERENCES

- Alexander M., 1973, *Astrophysics and Space Science*, 23, 459  
 Bell J., Bessell M., Stappers B., Bailes M., Kaspi V., 1995, *The Astrophysical Journal Letters*, 447, L117  
 Goldreich P., Nicholson P. D., 1989, *Astrophysical Journal*, 342, 1079  
 Hurley J. R., Tout C. A., Pols O. R., 2002, *Monthly Notices of the Royal Astronomical Society*, 329, 897  
 Hut P., 1981, *Astronomy and Astrophysics*, 99, 126  
 Kumar P., Quataert E. J., 1998, *The Astrophysical Journal*, 493, 412  
 Kushnir D., Zaldarriaga M., Kollmeier J. A., Waldman R., 2017, *Monthly Notices of the Royal Astronomical Society*, 467, 2146  
 Lai D., 1996, *The Astrophysical Journal Letters*, 466, L35  
 Murray C. D., Dermott S. F., 1999, *Solar system dynamics*. Cambridge university press  
 Savonije G., Papaloizou J., 1983, *Monthly Notices of the Royal Astronomical Society*, 203, 581  
 Storch N. I., Lai D., 2013, *Monthly Notices of the Royal Astronomical Society*, 438, 1526  
 Vick M., Lai D., Fuller J., 2017, *Monthly Notices of the Royal Astronomical Society*, 468, 2296  
 Vigna-Gómez A., MacLeod M., Neijssel C. J., Broekgaarden F. S., Justham S., Howitt G., de Mink S. E., Mandel I., 2020, *arXiv preprint arXiv:2001.09829*  
 Zahn J.-P., 1975, *Astronomy and Astrophysics*, 41, 329

This paper has been typeset from a  $\text{\LaTeX}$  file prepared by the author.